HHS Public Access

Author manuscript

Nanomedicine. Author manuscript; available in PMC 2015 August 01.

Published in final edited form as:

Nanomedicine. 2014 August ; 10(6): 1121–1130. doi:10.1016/j.nano.2014.03.004.

Gold Nanoparticles and Radiofrequency in Experimental Models for Hepatocellular Carcinoma

Mustafa Raoof, MD[1,*], **Stuart J. Corr, PhD**[1,2,*], **Cihui Zhu**[1], **Brandon T. Cisneros**[1,2], **Warna D Kaluarachchi, MS**[1], **Sophia Phounsavath**[1,2], **Lon J. Wilson, PhD**[2], and **Steven A. Curley, MD**[1,3]

[1]Department of Surgical Oncology, The University of Texas M. D. Anderson Cancer Center, Houston, TX, USA

[2]Department of Chemistry and Richard E. Smalley Institute for Nanoscale Science & Technology, Rice University, Houston, TX, USA

[3]Department of Mechanical Engineering and Materials Science, Rice University, Houston, TX, USA

Abstract

Hepatocellular carcinoma (HCC) is one of the most lethal and chemo-refractory cancers, clearly, alternative treatment strategies are needed. We utilized 10nm gold nanoparticles as a scaffold to synthesize nanoconjugates bearing a targeting antibody (cetuximab, C225) and gemcitabine. Loading efficiency of gemcitabine on the gold nanoconjugates was 30%. Targeted gold nanoconjugates in combination with RF were selectively cytotoxic to EGFR expressing Hep3B and SNU449 cells when compared to isotype particles with/without RF ($p<0.05$). In animal experiments, targeted gold nanoconjugates halted the growth of subcutaneous Hep3B xenografts in combination with RF exposure ($p<0.05$). These xenografts also demonstrated increased apoptosis, necrosis and decreased proliferation compared to controls. Normal tissues were unharmed. We have demonstrated that non-invasive RF-induced hyperthermia when combined with targeted delivery of gemcitabine is more effective and safe at dosages ~275-fold lower than the current clinically-delivered systemic dose of gemcitabine.

Keywords

Gemcitabine; Hyperthermia; radiofrequency; nanoparticle; hepatocellular

Corresponding author: Steven A. Curley, M.D., 1400 Holcombe Blvd, Unit 1484, Houston, TX 77230-1402, scurley@mdanderson.org, Phone: 713-794-4957, Fax: 713-745-5235.

*Equal Contribution

The authors disclose no potential conflicts of interest

INTRODUCTION

Cancer cell targeted drug delivery that minimizes toxicity and maximizes therapeutic benefit remains a fundamental challenge for successful cancer therapy. Over the past decade emerging nanotechnologies have shown promise in conquering barriers to transport of chemotherapeutic and biologic agents to malignant tissue while sparing normal organs. Nanoparticle-based combination therapies are of particular interest. However, translation of these systems to the clinic has been slow. The aim of the present study is to devise a EGFR-targeted non-invasive chemo-thermo-therapy that can be readily translated to the clinic by taking advantage of recent advances in our understanding of a) targeted drug delivery and b) thermal therapy of cancers. The premise of such work is based on the synergistic interaction of conventional cytotoxic chemotherapeutic agents and hyperthermia (1). We chose to direct our efforts at hepatocellular carcinoma (HCC) because conventional strategies have failed to provide relevant survival benefit and are too toxic in the majority of patients who also have concomitant underlying hepatic dysfunction (2). Challenges in advanced HCC treatment, therefore, exemplify the currently unmet need for novel, less toxic, and more effective strategies.

A growing body of experimental and theoretical work has demonstrated that metallic or semiconducting nanoparticles heat in an electromagnetic field, i.e. a near-infrared (NIR) or radiofrequency (RF) field (3–8). While NIR penetration in human tissues is limited to a few centimeters, shortwave RF fields in the megahertz range offer the benefit of full-body penetration. Prior *in vitro* and *in vivo* studies have demonstrated that this RF field-based nanohyperthermia system is safe and effective in a rabbit model of liver cancer after direct intra-tumoral injection of single-walled carbon nanotubes, and demonstrated efficacy without toxicity after systemic delivery of EGFR-targeted gold nanoparticles (AuNPs) in a mouse model of pancreatic adenocarcinoma (5, 6). In regards to cancer specific-targeted drug delivery, the list of conventional chemotherapeutic drugs that have been delivered using nanoparticles continues to grow and are reviewed elsewhere (9–11). Of these nanovectors, AuNPs are most extensively studied because they are already in clinical use and their physiochemical properties allow for a multitude of possible chemical linkages to targeting agents. For instance, Patra *et al*. successfully delivered gemcitabine non-covalently conjugated to AuNPs along with a targeting antibody (cetuximab, C225) against epidermal growth factor receptor (EGFR) in pancreatic adenocarcinoma cells (12).

Given these findings, we hypothesized that carefully-designed nanoparticles bearing a targeting antibody and a chemotherapeutic agent could be systemically delivered to human HCC xenografts. Upon delivery these conjugates would undergo pH-responsive release of the drug. Subsequent non-invasive RF induced-hyperthermia would then enhance tumor cell death because of the presence of drug and/or nanoparticles.

MATERIALS AND METHODS

Cell lines and Reagents

All cell lines (Hep3B, HepG2, SNU182, SNU475, SNU398 and SNU 449) were purchased from the American type culture collection (ATCC) and maintained as per the instructions of

the supplier. The short tandem repeat fingerprint was confirmed by the Cell Line Characterization Core Service (M. D. Anderson Cancer Center, Houston, TX) within one year of the experiments. Standard cell culture coated 12- and 24-well plates were used for experiments (Corning Inc., Corning, NY). Cetuximab (C225, Bristol-Myers Squibb, New York, NY), a chimeric monoclonal IgG_1 antibody against human EGFR-1, gemcitabine (Eli Lilly, Indianapolis, IN), the heterobifunctional alkane monothiol linker SPT-0012 (Sensopath Technologies, Inc., Bozeman, MT), mPEG-SH (Nanocs, New York, NY), and 10nm spherical AuNPs (Ted Pella, Inc., Redding, CA) were used in synthesizing the gold nanoconjugates. For immunohistochemistry, mouse anti-human Ki67 (M7240, Dako, Carpinteria, CA), rabbit anti-cleaved caspase 3 (Asp175, Cell Signaling, Danvers, MA) and rat anti-BrdU (Abcam, Cambridge, MA) were used. Rat and mouse primary antibodies were detected using a HRP/Polymer kit from Biocare, while rabbit antibodies were detected using Envision+/HRP from Dako (Carpinteria, CA)

Synthesis and characterization of gold conjugates

Gold nanoconjugates were synthesized as described in detail previously with some modifications that are discussed here (6, 13). The stock buffer from as purchased citrate-capped AuNPs was exchanged with a borate buffer (Sigma-Aldrich, St. Lous, MO) using 50kDa centrifugation filter (50 kDa, Amicon, Milipore, Billerica, MA). Gemcitabine was added to 50 μg/ml aliquots of AuNPs in borate buffer to a final gemcitabine concentration of 0 to 100 μg/ml and incubated for a variable duration. Incubation of 50 μg /ml AuNP with 10 μg/ml gemcitabine for 1 hour was optimal and was used for subsequent conjugations. Cetuximab (C225) was separately modified using a heterobifunctional alkane linker as described elsewhere (6, 13). This modified antibody was then added to AuNP-gemcitabine conjugates (30 μg of C225-linker to 50 μg Au in each ml of reaction mixture, to obtain AuNP-C225-gemcitabine (ACG) nanoparticles (2–3 h incubation at room temperature). The conjugates were further modified using methoxypoly(ethylene glycol)-thiol (mPEG-SH) at a final concentration of 100uM in the reaction mixture for 1 hour to yield AuNP-C225-gemcitabine-mPEG (ACGP) nanoparticles. Successful conjugation and stability after 150 mM NaCl challenge was analyzed at each step using UV-Vis spectroscopy (Applied Nanofluorescence, Houston, TX) and dynamic light scattering (Malvern Instruments, Westborough, MA). Finally, the gold nanoconjugates were purified using filter centrifugation (50 kDa, Amicon, Milipore, Billerica, MA) to remove excess unconjugated gemcitabine and mPEG-SH. Isotype control AuNP-IgG-gemcitabine-mPEG (AIGP) nanoparticles were synthesized similarly by using isotype control human IgG in place of C225. Gemcitabine loading was determined by measuring unbound gemcitabine that was removed after filter centrifugation using reverse phase high performance liquid chromatography (HPLC) described elsewhere (14). Briefly, the UV absorbance of chromatographic peaks was recorded (Waters 1525 HPLC system, Milford, MA) at 275nm after separation through a Phenomenex Luna 5uC18(2) 100A column (250 x 4.6 mm, particle size 5 microns silica) using 0.1% TFA-water/acetonitrile at ambient temperature. A standard curve of area-under-the-curve corresponding to a gemcitabine elution fraction was generated using known concentrations and unknown concentrations were determined.

In order to understand the release kinetics of gemcitabine from these conjugates, ACGP nanoparticles were centrifuged at 13,200 RPM for 30 minutes to remove unbound C225, gemcitabine, and mPEG. The pellet was resuspended in a physiologic buffer (PBS+1g/dL bovine serum albumin) and aliquoted into several tubes. At each time point over the course of 24 hours, the colloidal suspension in the physiologic media was centrifuged at 13200 RPM for 1 hour to pellet all the ACGP conjugates; the supernatant was removed and analyzed by HPLC. The gemcitabine concentration was determined by comparing to a known standard. These experiments were repeated at pH 5, pH 6 and with or without non-invasive RF field exposure (600 W, 13.56 MHz, one minute duration). To assess the conjugation of C225-L to AuNPs, we labeled C225-L with AlexaFluor-647 fluorophore, as previously described (15). Briefly, after incubating AuNPs with a known concentration of C225-L, the conjugates were pelleted. Fluorescence was measured in the supernatant and C225-L concentration quantified against a standard scale. We estimated 600ng of C225-L on each microgram of AuNP.

In vitro studies

Flow cytometry was performed using a BD LSR II FACS unit (BD Biosciences, San Jose, CA). After trypsinization, approximately 1 million cells were incubated on ice with phycoerytherin (PE)- conjugated EGFR antibody or isotype control (BD Biosciences, San Jose, CA) for 30 minutes. Subsequently, the cells were resuspended in PBS and washed twice before analyzing with the FACS analysis (Excitation: 561nm, Emission: 570–597nm).

For inductively coupled plasma atomic mass spectrometry (ICP-MS), approximately 1 million cells in adherent sub-confluent monolayers were incubated with targeted or isotype gold nanoconjugates (at Au concentration of 0.2 mg/ml) for 4 hours. The samples were washed twice with PBS and trypsinized. Cell pellets were digested with aqua regia (1 part nitric acid and 3 parts hydrochloric acid by volume). The gold concentration was determined using a Perkin Elmer Elan 9000 (Waltham, MA) ICP-MS instrument, as per manufacturer's instructions.

Transmission electron microscopy (TEM) studies were performed as described previously (15). For cytotoxicity studies, exponentially-growing adherent monolayers were exposed to the varying conditions as mentioned in the text with or without RF exposure in a 12-well plate. Nanoparticles were administered by gold concentration at 0.2 mg/ml. The Kanzius RF generator set-up for *in vitro* studies has been described previously (15). Briefly, cells were plated in three adjacent wells of a 12-well plate. The plates were positioned on a Teflon holder in the RF field such that there was a uniform RF field across the three wells. The bulk media temperature remained <37°C for the exposure duration of 4.5 minutes. This value was determined to be LD_{75} of RF exposure for both cell lines under the stated conditions. Viability was measured using a standard MTT assay as a percentage of untreated controls.

In vivo studies

All mice were kept in accordance with an Institutional Animal Care and Use Committee approved protocol. A mouse model of liver cancer was generated using subcutaneous implantation of approximately 3 million cells in the dorsal midline of 4wk old BalbC/ Nu

mice. The cells were injected in a 200 μl final volume, mixed with matrigel (1:1 v:v), and mice were randomized to one of 5 groups as stated in the text (7 mice per group). After three weeks, the mice that did not form tumors were excluded. At this point the greatest tumor dimension (either height, width or length) of each group was ~0.5 cm. Animals were injected with or without gold nanoconjugates (AuNP concentration 10 mg/kg) systemically (intraperitoneal, IP) approximately 24 hours prior to RF exposure. This treatment was repeated twice a week and was continued over three weeks with mice receiving a total of six doses. For RF treatment, the mice were placed on the Rx head of the *in vivo* RF generator under anesthesia and grounded using a copper tape, as described previously (6). The temperature of the ectopic tumor was monitored continuously using an infrared (IR) thermal camera (FLIR SC 6000, FLIR Systems, Inc., Boston, MA). RF exposures were paused when the surface tumor temperature reached 43°C and were then resumed at 40°C for a total "RF on" duration of 10 minutes. A stock AuNP solution was used as an internal control to ensure calibration between RF exposures. Tumor volumes were calculated using the formula for an ellipsoid (π x length x width x height /6). Animals were sacrificed 24 hours after the last RF treatment or 48 hours after the last dose of nanoparticles. Tumors were harvested from all the mice and weighed. We administered 10 mg/kg BrdU (i.p.) 24 hours before sacrificing the animals. Tumors and other organs were harvested for mass determination, histological analysis, or ICP-MS. Specimens for ICP-MS were washed with PBS, wiped dry, weighed and then subjected to slow acid digestion as described above for *in vitro* studies. The gold concentration of each sample was determined by ICP according to the manufacturer's recommendations (iCAP 6500, Thermo Fisher Scientific, Waltham, MA). For Au plasma level determination, blood was collected from the mandibular vein of live animals and intra-cardiac puncture for terminal animals under isoflurane anesthesia.

For histological analysis, samples were formalin fixed and paraffin embedded. Five-micron sections were placed on unstained slides. Subsequent processing (H&E staining and immunohistochemistry, IHC) was performed on a Dako automated stainer as a single batch per antigen. For IHC, primary antibodies were detected using a colorimetric DAB stain. Three random high power fields (10 x objectives) were analyzed from a single section across the middle of each tumor. At least 3 tumors were analyzed per group on a multispectral scope (Olympus IX51 featuring a CRi Nuance camera, Hopkinton, MA). Staining was quantified using inForm™ (CRI, Capillary Life Sciences, Hopkinton, MA); pattern recognition software that subjects multispectral data to machine-learning algorithms for accurate quantification of staining.

Statistical Methods

Results are reported as mean±SEM unless otherwise noted. For all inferential statistics, null hypothesis was rejected at $p<0.05$. Two-sided student's t-test was used for two-group means. Multiple group comparisons were performed using one-way ANOVA. All data was plotted and analyzed in Prism 5.0 La Jolla, CA

RESULTS

Characterization of gold nanoconjugates

Size distribution of as-purchased 10nm citrate-capped AuNPs was confirmed by TEM and DLS (Figure 1D). The kinetics of gemcitabine loading onto the AuNPs was evaluated using UV-Vis spectroscopy. Citrate-capped AuNPs in borate buffer (50 μg/ml) demonstrated concentration- and time-dependent gemcitabine loading as suggested by a red-shift in the peak surface-plasmon resonance (SPR). Prolonged incubation, as well as a higher concentration of gemcitabine, led to aggregation of AuNPs (Figure 1A and 1B). The optimal concentration of gemcitabine and duration of its incubation with AuNPs was found to be 10 μg/ml and 1-hour, respectively. Addition of C225 antibody conjugated to a linker lead to a further slight red-shift in the peak SPR confirming conjugation without aggregation (Figure 1C). The surface of the ACG nanoconjugates was further passivated with 5 kDa mPEG-SH to prevent non-specific interactions as well as to avoid immune recognition. This increased the median hydrodynamic diameter from 50 nm (without mPEG) to 68 nm (with mPEG) (Figure 1D). The ACGP conjugate hence formed was stable after adding 150mM NaCl in 1:1 (v:v) ratio (Figure S1A). Finally, the loading efficiency of gemcitabine in this conjugate was found to be 30%, as determined by HPLC, corresponding to a Gemcitabine:AuNP (w:w) ratio of 6%.

Stability of ACGP conjugates was also tested and confirmed in buffer solution with increasing protein concentration (Figure S1B). We found that gemcitabine was released in a pH-dependent (Figure 1E), but RF-independent manner (Figure S2A). Of the total bound, 28.8 ± 0.4% of the gemcitabine was released at pH 6 as opposed to 8.8±0.2% at pH 7.4 after 24 hours ($p<0.05$). This pH-dependent release was due to aggregation of the AuNPs as demonstrated by a >10 nm shift in peak SPR and broadening of the peak by UV-Vis spectroscopy (Figure 1D), along with dissociation of the C225 antibody from the AuNP surface (Figure S2B). After confirming stability, loading, and release of gemcitabine in a pH-responsive manner, we evaluated the heating of these conjugates in the RF field. We found that ACG and ACGP nanoconjugates did not heat above the background buffers (Figure S3).

Gold nanoconjugate uptake and cancer cell specific cytotoxicity *in vitro*

Despite the lack of heating from gold gemcitabine nanoconjugates in the RF field, we proceeded with the evaluation of these conjugates *in vitro* and *in vivo*. We reasoned that because of previously reported synergy between gemcitabine and hyperthermia, tissues that contain gemcitabine would be preferentially susceptible to the effects of RF-induced hyperthermia.

First, we evaluated cell surface EGFR-1 expression in a panel of six hepatocellular carcinoma cell lines using flow cytometry (Figure 2A). It was noted that SNU449 cells had the highest expression of EGFR-1 41.5± 6.7% (mean± SD). This was closely followed by the Hep3B cell line, 36.8±4.2%. In contrast, EGFR-1 expression was negligible in the HepG2 cell line. Given these findings, we evaluated ACGP uptake in the two EGFR-1-high cell lines and one EGFR-1-low cell line. The mechanism of uptake of anti-EGFR-coated

AuNPs has previously been described in detail (6, 16). The internalization is rapid with most of the surface bound conjugates internalized within one hour. We utilized ICP-MS and TEM to quantitatively and qualitatively assess the uptake of these nanoconjugates by liver cancer cells, respectively (Figure 2B and 2C). We note that ACGP nanoparticles are internalized and localized to an endolysosomal compartment after 4 hours of incubation, while cells incubated with isotype control AIGP nanoparticles were rarely seen to have internalized the nanoconjugates. The amount of Au internalized is reported in Figure 2B on a per-cell basis. These results demonstrate selective cell surface receptor-based internalization of conjugates by cancer cells after 4 hours of incubation. In contrast, uptake of ACGP or AIGP nanoparticles in EGFR-1-low HepG2 cells could not be detected by ICP-MS.

Next, we inquired if RF exposure of cancer cells that have selectively internalized gemcitabine-loaded nanoparticles enhanced targeted cell killing. For this purpose, we evaluated cytotoxicity using the standard MTT assay. We found that for the SNU449 cell line (Figure 2D), control cells that were untreated or treated with isotype nanoparticles or an equimolar dose of gemcitabine (12μg/ml) for 4 hours showed no cytotoxicity. However, ACGP nanoparticles demonstrated significant cytotoxicity compared to controls ($p<0.05$). We exposed these groups to 4.5 min of RF exposure (Kanzius RF generator, 13.56 MHz, 600 W). This dose was found to yield ~LD_{25} in cells treated with RF alone. We note that the group that received the combination treatment with targeted nanoparticles for 4 hours, followed by RF exposure for 4.5 min, demonstrated the highest cytotoxicity, while the other RF groups were not significantly different from the RF alone group. Similar results were noted with experiments conducted on Hep3B cells that demonstrated EGFR-1-targeted gemcitabine cytotoxicity was further enhanced by RF field exposure (Figure 2E). Similar experiments conducted on EGFR-1-low HepG2 cells failed to show significant toxicity in combination therapy group compared to control groups (Figure 2F).

Chemosensitization of HCC xenografts by RF field exposure after gold nanoconjugate administration

A human liver cancer model was generated in a mouse subcutaneously implanted with EGFR-expressing Hep3B cells (Figure 3A) in the dorsal midline. The ectopic location of the tumor allowed easy control over thermal dosimetry by monitoring the temperature of the tumor in real-time using an IR thermal camera when the mouse was placed in an RF field (Figure 3B). Mice were randomized to one of five groups (Untreated, RF field exposure only, ACGP only, AIGP + RF, and ACGP + RF). As demonstrated in Figure 3C, tumors in the combination group with targeted nanoconjugates showed delayed growth kinetics. We also found that RF treatment by itself did not have an impact on tumor growth, while tumors in other nonspecific treatment groups demonstrated intermediate response. Tumor mass data is summarized in Figure 3D. One mouse in the untreated group was sacrificed because of tumor burden at 11 days after the start of treatment and is not included in the final tumor mass analysis. Figure 3D demonstrates that mice that were treated with ACGP followed by RF field exposure had the smallest tumors, which was significantly different from the control group ($p=0.0003$). Mice treated with ACGP alone or mice treated with AIGP followed by RF were smaller than the control group, however this did not reach statistical significance. To address the question if antibody targeting had an effect on anti-tumor

efficacy, we compared the tumor mass of mice treated with ACGP followed by RF with their isotype counterparts. We found that mice in the former group had tumors that were significantly smaller than the mice in the latter group (p=0.015). We further asked if RF exposure had any added value to the mice treated with ACGP. We found that although the mean tumor mass of the mice treated with ACGP followed by RF (194±65) was less than half of the mice treated with ACGP alone (486±164 mg), it did not reach statistical significance (p=0.13).

Detailed histological analysis was then performed on the tumor tissues and viscera to assess molecular markers of response as well as to assess toxicity (Figure 4 and Figure S4). Tumor necrosis, as assessed by routine H&E staining, demonstrated that the RF treated groups generally had a 2–3 fold higher necrosis rate than other groups. However, this was not significant in multiple comparison tests. Tumors of mice treated with ACGP demonstrated a 15-fold increase in apoptosis compared to untreated controls ($p<0.05$). Since gemcitabine is incorporated into the DNA and inhibits DNA synthesis, we wanted to quantify this effect in the tumor tissues. Twenty-four hours before sacrifice and immediately after the last RF exposure, mice were given BrdU 10 mg/kg IP (intra-peritoneal). The BrdU incorporation was measured in tissues, which provided a direct correlate of activity of gemcitabine in tissues. We observed that tumors treated with ACGP followed by RF had the lowest BrdU uptake compared to untreated controls. This was also confirmed using a marker of proliferation, Ki67, that demonstrated similar results.

We studied tumor accumulation and plasma levels after injecting a single intra-peritoneal dose of ACGP nanoparticles (at 10 mg/kg by gold concentration). We note that tumor accumulation increased over-time, reaching a plateau at 24–48 hours after injection (Figure S5). Similar dynamics were seen with accumulation in the liver and spleen. We find that 0.52% of the injected dose accumulates in the tumor, which is comparable to 1.02% of the dose accumulated in liver. This demonstrates that even though nanoparticles are cleared by the reticuloendothelial system, significant AuNPs accumulate in the tumor tissue.

We asked if changing the route of administration could prevent the enhanced accumulation in the reticuloendothelial system. For that purpose, ACGP nanoparticles were injected in the tail vein or via an intra-peritoneal route. We noted that the Au plasma levels peak 15-min after intravenous injection was 6.7±1 mg/L and one-hour after intra-peritoneal injection was 0.23±0.1 mg/L (Figure S5). This was followed by a prolonged clearance lasting more than 24 hours. The area-under-curve for the two routes was comparable, i.e. 23.6 mg.h/L and 15.7 mg.h/L (p=0.67) for intravenous and intraperitoneal injection, respectively. We note that 24 hours after injection, the levels of Au accumulated in liver tissue are not significantly different for either route. However, after intraperitoneal injection a significantly higher accumulation of ACGP nanoparticles is seen in the spleen compared to the intravenous administration (p=0.024). These findings suggest that intravenous administration of ACGP nanoparticles can partially prevent their clearance by the reticuloendothelial system in comparison to intraperitoneal administration.

In order to assess the safety of this modality, mice were monitored closely throughout the study. Histological analysis did not demonstrate any damage to native viscera in the

treatment groups. BrdU uptake in the spleen and intestine was similar for all groups treated, suggesting minimal effect on proliferation of these tissues following treatment with the nanoconjugates with or without RF field exposure (Figure S6).

DISCUSSION

In this series of experiments, we have demonstrated the pre-clinical activity of a carefully-designed nanoconjugate, ACGP, in combination with brief (10 min) high intensity (600 W) shortwave RF field exposure against human HCC cell lines and tumors with moderate over-expression of the target (EGFR-1). This conjugate comprised of several components each with an important function, as described below.

Firstly, the AuNP platform was chosen since nanotoxicology studies in small and large animals have failed to show any toxicity at a macroscopic as well as a molecular level (17, 18). AuNPs also act as susceptors in a shortwave RF-field (3, 4, 6, 8), are easily functionalized with targeting moieties or drugs (9–12), and can be synthesized in a reproducible and cost-effective manner. Despite their accumulation in the liver (Kupffer cells), we found that these AuNPs do not harm liver parenchyma or other viscera, which is consistent with prior observations (6, 17). We have previously shown that AuNPs are predominantly eliminated by renal clearance and their elimination, therefore, should be independent of hepatic dysfunction(17). In regards to the choice of drug for conjugation, we were limited; conventional cytotoxic chemotherapies have failed to be of much benefit with a median survival of 7–8 months for advanced HCC which is extended for only three more months by use of the multiple kinase inhibitor sorafenib (2). Several factors led us to select gemcitabine for this purpose. A 17% response rate with gemcitabine was seen as a single agent in, at least, one study of patients with advanced HCC. Gemcitabine and its metabolite are renally cleared and it is tolerated well in these patients (19). Moreover, gemcitabine is heat stable and has known synergy with hyperthermia that has previously been well characterized in rodent models of lung cancer and rhabdomyosarcoma (20, 21). Very few targets have been identified in HCC that have translational relevance. We used cetuximab (C225) because surface EGFR-1 over-expression is associated with late stage disease and it is found in 66% of human HCC tumors, making it a potential target (22). It is also FDA approved for use in other solid tumors. We used a heterobifunctional linker for conjugation. From prior studies, we understood that gold nanoconjugates when prepared using this linker, are internalized by receptor-mediated endocytosis and within 30 min – 4 hours are found in late endosomes and lysosomes within the targeted cancer cells (15). Intracellular pH measurements around these AuNPs demonstrated that this pathway involves a transition from pH 7.4 in the serum to pH 5.5 or less in the lysosomes. This leads to aggregation of the AuNPs and dissociation of C225. In the experiments reported here, we further showed that gemcitabine unloading is enhanced in a pH dependent manner from this construct, thereby triggering only intracellular release. We were limited in quantifying the release of gemcitabine inside cancer cells by the lack of readily-available methods to detect intracellular levels of gemcitabine. Because the nanoconjugates are stable in physiologic conditions, we make the assumption that AuNP biodistribution and pharmacokinetics are representative of gemcitabine. Finally, our intention was to design particles that would not only reach the tumor microvasculature, but would also extravasate and permeate throughout

the tumor microenvironment. It has previously been shown that particles <20 nm extravasate and permeate too quickly through the tumor while larger particles >80 nm do not permeate at all (23). Untargeted AuNPs that were 40–80 nm were found to accumulate within the tumor stroma more readily. The conjugates were therefore designed to be between 50–70 nm in this study.

For *in vitro* cell studies we administered these nanoconjugates to cancer cells for brief incubation periods mimicking fixed dose rate regimens of gemcitabine (e.g 10 mg/m2/min for 100 min resulting in ~15 uM peak plasma concentration). A much higher dose of gemcitabine (40 uM) for a much longer duration (4 hours) did not result in significant cytotoxicity compared to controls in either cell line when analyzed 24 hours later. Our results demonstrated that the same gemcitabine dose when delivered after conjugation to AuNPs results in much higher cytotoxicity against HCC cells. We further demonstrated that RF exposure, following internalization of gemcitabine-loaded gold nanoconjugates, significantly enhanced cytotoxicity. Current clinically relevant dosages are in excess of 1000 mg/m2/wk (19). This translates to a mouse dose of 330 mg/kg/wk (FDA oncology dose calculator) (24). The gemcitabine dose used in the *in vivo* study was ~1.2 mg/kg/wk which is ~275-fold lower than the lowest clinically relevant dose. Since the majority of the injected dose of the gold nanoconjugates accumulates in liver and spleen, it is possible that (in addition to EGFR-targeted drug delivery) these conjugates act as *in vivo* depots of gemcitabine. In this regard, we demonstrated evidence that isotype control nanoconjugates were partly effective in combination with RF. However, we failed to find any toxic effects of gemcitabine in these organs. We note a very low proliferation rate in normal liver parenchyma from BrdU labeling experiments. Since gemcitabine is incorporated in the S-phase of the cell cycle, this may explain the liver sparing effect of the ACGP nanoparticles. The liver sparing effect could also be explained based on our previous observations that demonstrate Kupffer cells, but not hepatocytes to be the predominant site of accumulation of gold nanoparticles after systemic administration (6). These Kupffer cells are rapidly replaced from the systemic circulation and bone marrow without obvious consequence to liver parenchyma. Finally, our recent findings suggest that RF absorption and dissipation of heat in liver tumors is higher than normal liver parenchyma, which is predominantly due to the different electrical properties of the two types of tissue (25). All of these observations help explain the lack of toxicity to normal liver in comparison to liver tumor. Future studies will focus on evaluating how these findings can be translated to clinical scenarios because HCC frequently arises in the context of a cirrhotic liver.

The findings of this study should be interpreted with caution. The limitations of an ectopic tumor model are acknowledged. As more RF field compatible tools for orthotopic tumor thermography become available, the experiments need to be repeated in these more relevant orthotopic HCC models. Even though EGFR is over-expressed in 66% of human HCC, it is also expressed in a wide variety of normal tissues making it a relatively non-specific target. It is plausible that the use of EGFR-1-targeted nanoconjugates in human model could result in toxicity that is not observed in small animal models. We are currently evaluating more specific targets in HCC cells to determine the feasibility of this approach for human patients.

Taken together, these findings highlight a novel method that has far-reaching potential to deliver safe and effective combination therapies to patients with advanced HCC.

Supplementary Material

Refer to Web version on PubMed Central for supplementary material.

Acknowledgments

Funding sources: This work was funded from the NIH (U54CA143837), NIH M. D Anderson Cancer Center Support Grant CA016672, the Welch Foundation (Grant C-0627), the V Foundation (SAC), and an unrestricted research grant from the Kanzius Research Foundation (SAC, Erie, PA).

References

1. Field SB, Bleehen NM. Hyperthermia in the treatment of cancer. Cancer Treat Rev. 1979 Jun; 6(2): 63–94. [PubMed: 39673]
2. Llovet JM, Ricci S, Mazzaferro V, Hilgard P, Gane E, Blanc JF, et al. Sorafenib in Advanced Hepatocellular Carcinoma (vol 359, pg 378, 2008). New England Journal of Medicine. 2008 Dec 4.359(23):2508.
3. Cherukuri P, Glazer ES, Curleya SA. Targeted hyperthermia using metal nanoparticles. Advanced Drug Delivery Reviews. 2010 Mar 8; 62(3):339–45. [PubMed: 19909777]
4. Corr, SJ.; Raoof, M.; Phounsavath, S.; Cheney, MA.; Cisneros, B.; Mackeyev, Y.; Shur, M.; Gozin, M.; McNally, PJ.; Wilson, LJ.; Curley, SA. Size-, concentration-, and surface-dependent heating of gold nanoparticles in a radiofrequency electric-field. 2011. submitted
5. Gannon CJ, Cherukuri P, Yakobson BI, Cognet L, Kanzius JS, Kittrell C, et al. Carbon nanotube-enhanced thermal destruction of cancer cells in a noninvasive radiofrequency field. Cancer. 2007 Dec 15; 110(12):2654–65. [PubMed: 17960610]
6. Glazer ES, Zhu C, Massey KL, Thompson CS, Kaluarachchi WD, Hamir AN, et al. Noninvasive radiofrequency field destruction of pancreatic adenocarcinoma xenografts treated with targeted gold nanoparticles. Clin Cancer Res. Dec 1; 16(23):5712–21. [PubMed: 21138869]
7. Hanson GW, Patch SK. Optimum electromagnetic heating of nanoparticle thermal contrast agents at rf frequencies. Journal of Applied Physics. 2009 Sep 1.106(5)
8. Kruse DE, Stephens DN, Lindfors HA, Ingham ES, Paoli EE, Ferrara KW. A Radio-Frequency Coupling Network for Heating of Citrate-Coated Gold Nanoparticles for Cancer Therapy: Design and Analysis. Ieee Transactions on Biomedical Engineering. 2011 Jul; 58(7):2002–12. [PubMed: 21402506]
9. Ghosh P, Han G, De M, Kim CK, Rotello VM. Gold nanoparticles in delivery applications. Advanced Drug Delivery Reviews. 2008 Aug 17; 60(11):1307–15. [PubMed: 18555555]
10. Mandal S, Bakeine GJ, Krol S, Ferrari C, Clerici AM, Zonta C, et al. Design, development and characterization of multi-functionalized gold nanoparticles for biodetection and targeted boron delivery in BNCT applications. Applied Radiation and Isotopes. 2011 Dec; 69(12):1692–7. [PubMed: 21641810]
11. Pissuwan D, Niidome T, Cortie MB. The forthcoming applications of gold nanoparticles in drug and gene delivery systems. Journal of Controlled Release. 2011 Jan 5; 149(1):65–71. [PubMed: 20004222]
12. Patra CR, Bhattacharya R, Wang EF, Katarya A, Lau JS, Dutta S, et al. Targeted delivery of gemcitabine to pancreatic adenocarcinoma using cetuximab as a targeting agent. Cancer Research. 2008 Mar 15; 68(6):1970–8. [PubMed: 18339879]
13. Kumar S, Aaron J, Sokolov K. Directional conjugation of antibodies to nanoparticles for synthesis of multiplexed optical contrast agents with both delivery and targeting moieties. Nature Protocols. 2008; 3(2):314–20.

14. Lanz C, Fruh M, Thormann W, Cerny T, Lauterburg BH. Rapid determination of gemcitabine in plasma and serum using reversed-phase HPLC. Journal of Separation Science. 2007 Aug; 30(12): 1811–20. [PubMed: 17638352]
15. Raoof M, Corr SJ, Kaluarachchi WD, Massey KL, Briggs K, Zhu C, et al. Stability of antibody-conjugated gold nanoparticles in the endo-lysosomal nanoenvironment: Implications for non-invasive radiofrequency-based cancer therapy. Nanomedicine. Feb 17.
16. Bhattacharyya S, Bhattacharya R, Curley S, McNiven MA, Mukherjee P. Nanoconjugation modulates the trafficking and mechanism of antibody induced receptor endocytosis. Proceedings of the National Academy of Sciences of the United States of America. 2010 Aug 17; 107(33): 14541–6. [PubMed: 20679244]
17. Glazer ES, Zhu C, Hamir AN, Borne A, Thompson CS, Curley SA. Biodistribution and acute toxicity of naked gold nanoparticles in a rabbit hepatic tumor model. Nanotoxicology. Dec; 5(4): 459–68. [PubMed: 20854190]
18. Higby GJ. Gold in medicine: a review of its use in the West before 1900. Gold Bull. 1982; 15(4): 130–40. [PubMed: 11614517]
19. Yang TS, Lin YC, Chen JS, Wang HM, Wang CH. Phase II study of gemcitabine in patients with advanced hepatocellular carcinoma. Cancer. 2000 Aug 15; 89(4):750–6. [PubMed: 10951336]
20. Van Bree C, Beumer C, Rodermond HM, Haveman J, Bakker PJM. Effectiveness of 2′, 2′ difluorodeoxycytidine (Gemcitabine) combined with hyperthermia in rat R-1 rhabdomyosarcoma in vitro and in vivo. International Journal of Hyperthermia. 1999 Nov-Dec;15(6):549–56. [PubMed: 10598951]
21. Vertrees RA, Das GC, Popov VL, Coscio AM, Goodwin TJ, Logrono R, et al. Synergistic interaction of hyperthermia and gemcitabine in lung cancer. Cancer Biology & Therapy. 2005 Oct; 4(10):1144–53. [PubMed: 16138007]
22. Buckley AF, Burgart LJ, Sahai V, Kakar S. Epidermal growth factor receptor expression and gene copy number in conventional hepatocellular carcinoma. Am J Clin Pathol. 2008 Feb; 129(2):245–51. [PubMed: 18208805]
23. Perrault SD, Walkey C, Jennings T, Fischer HC, Chan WCW. Mediating Tumor Targeting Efficiency of Nanoparticles Through Design. Nano Letters. 2009 May; 9(5):1909–15. [PubMed: 19344179]
24. FDA: Oncology tools- Dose Calculator. Feb 21. 2013 Available from: http://www.accessdata.fda.gov/scripts/cder/onctools/animalquery.cfm
25. Raoof M, Cisneros BT, Corr SJ, Palalon F, Curley SA, Koshkina NV. Tumor selective hyperthermia induced by short-wave capacitively-coupled RF electric-fields. PLoS One. 2013; 8(7):e68506. [PubMed: 23861912]

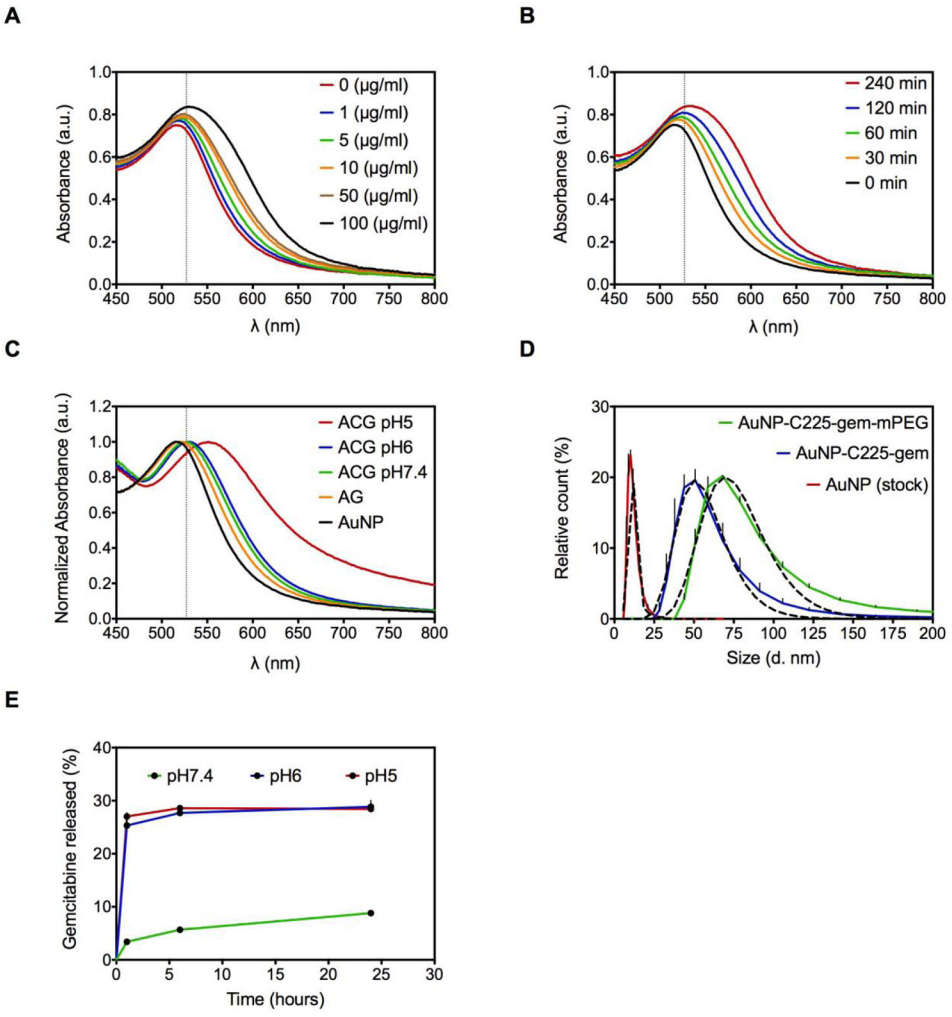

Figure 1. Synthesis and characterization of gold nanoconjugates

(A) Gemcitabine was loaded onto AuNPs (50 μg/ml) by passive conjugation at varying concentrations and UV-Vis spectra were analyzed at 1 hour after incubation at RT. (B) Fixed concentration (10 μg/ml) of gemcitabine was incubated with AuNPs (50 μg/ml) and UV-Vis spectra were analyzed at varying time points. (C) UV-Vis spectra demonstrating red-shift in AuNP SPR with stepwise addition of gemcitabine (10 μg/ml) for 1 hour and C225 (30 μg/ml) for 2 hours. A decrease in pH from 7.4–5 leads to aggregation of these nanoconjugates. (D) Hydrodynamic diameter distribution of stock AuNPs and final conjugates with and without mPEG-SH. Solid lines represents experimental observation and dashed lines represent curve-fit values from a Gaussian (log) distribution. (E) Release of gemcitabine from gold nanoconjugates is analyzed by RP-HPLC as detailed in methods at varying pH. For A,B,C, vertical dashed line represents a 10 nm shift from peak SPR of unconjugated AuNP. Peak SPRs to the right of this line along with broadening of the peak is evidence of aggregation.

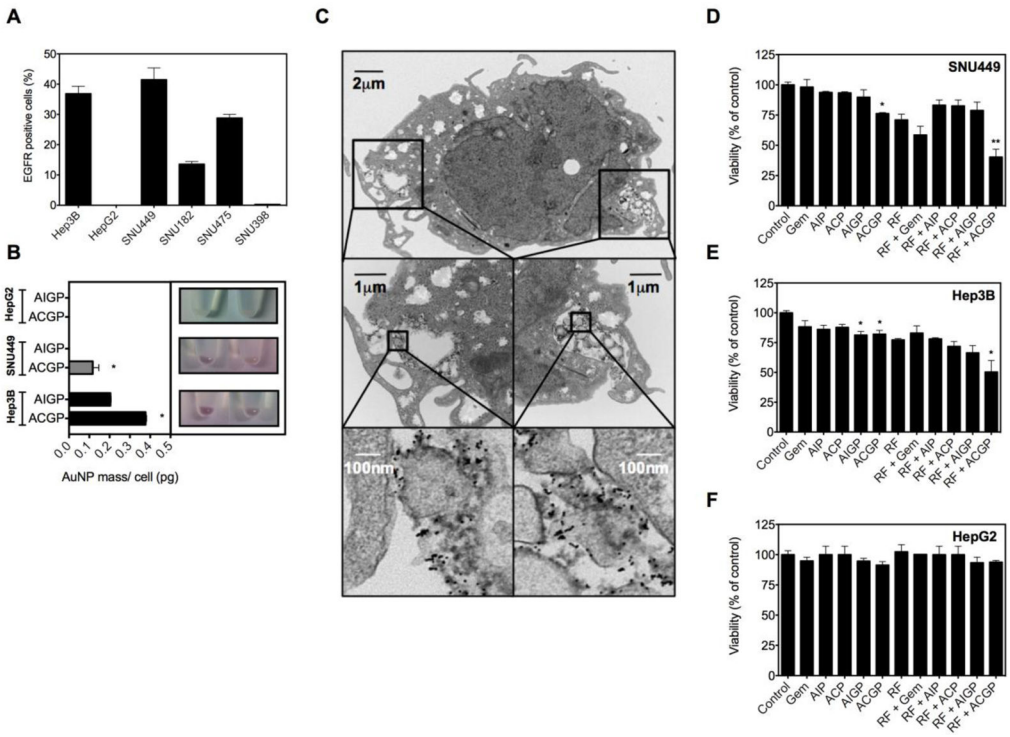

Figure 2. Gold nanoconjugate uptake and cytotoxicity in combination with RF-induced hyperthermia *in vitro*

(A) EGFR expression was analyzed in a panel of 6 human HCC cell lines by flow cytometry. (B) Gold uptake is quantified using ICP-MS in Hep3B, SNU449 or HepG2 cells pre-treated with ACGP particles or isotype control AIGP particles (n=3, *p<0.001 vs. isotype control). (C) Uptake of ACGP conjugate by Hep3B liver cancer cells after 4 hours of incubation. (D, E, F) Hep3B, SNU449 or HepG2 cells were incubated with or without gold nanoconjugates bearing gemcitabine or equimolar gemcitabine for 4 hours followed by RF exposure for 4.5 min. Cytotoxicity was analyzed 24 hours later using MTT assay (n=3–6, *p<0.05 vs. control for no RF groups and vs. RF alone for RF treated groups). *AuNP-C225-mPEG (ACP); AuNP-IgG-mPEG (AIP); AuNP-C225-gem-mPEG (ACGP); AuNP-IgG-gem-mPEG (AIGP); Gemcitabine (Gem)*

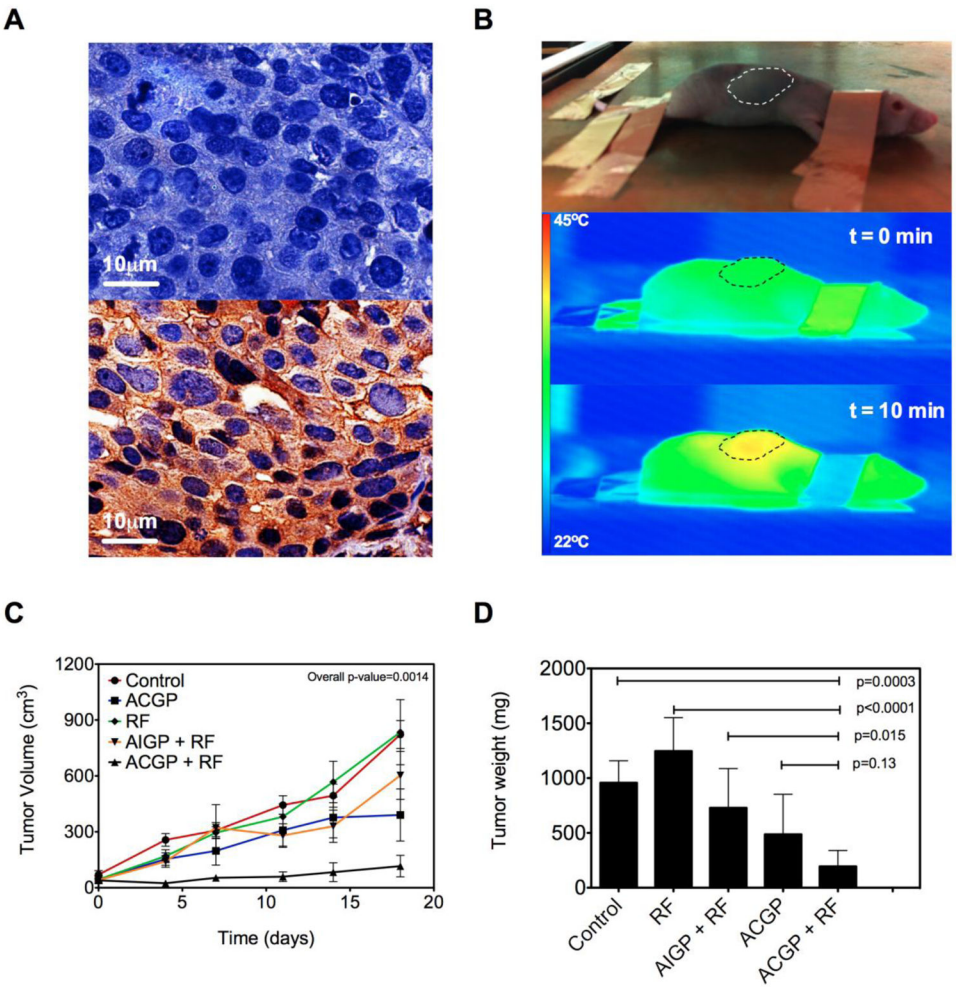

Figure 3. Effectiveness of gold nanoconjugates in combination with RF *in vivo*

(A) Cell-surface EGFR expression in Hep3B xenografts (bottom) in comparison with DAB staining control (top). (B) A BalbC/Nu mouse is sedated and placed in an RF field on copper ground plate (Rx head) ~2 inches from Tx head (not shown). Animals are connected to the ground using copper tape to prevent electrothermal injury. Tumor temperature is monitored in the reference frame and thermal dose titrated. (C) Changes in tumor volume are recorded after the start of treatment at day 0. (n=5–7, Overall p-value from One-way ANOVA) (D) Tumor mass was documented 24 hours after last RF treatment or 48 hours after last nanoparticle treatment (Mean SD). *AuNP-C225-gem-mPEG (ACGP); AuNP-IgG-gem-mPEG (AIGP).*

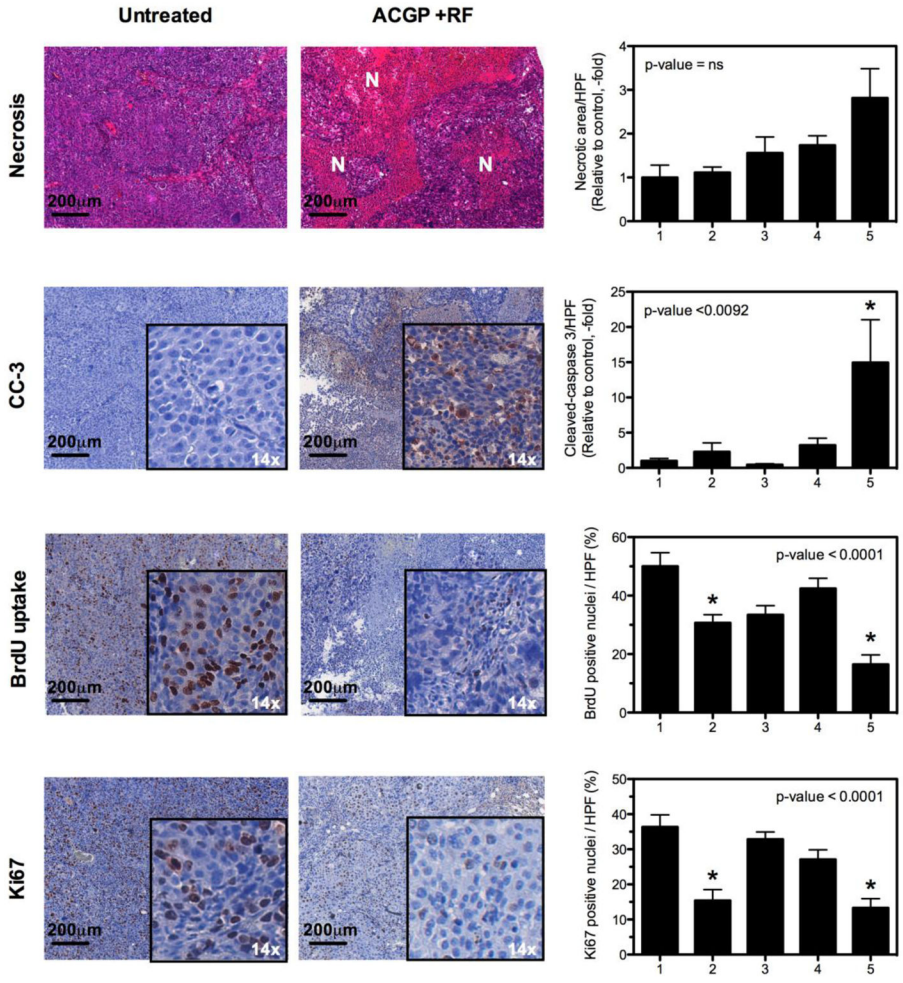

Figure 4. Histological analysis of tumor tissues

Tumors harvested at the end of experiment were analyzed. Three random images were taken from each tumor. At least 3 tumors from each group were analyzed. Colorimetric staining and necrosis was quantified using CRI-Nuance multispectral microscope and inForm software. *(p-values from one-way ANOVA, * represent level of significance at $p<0.05$ from Dunn's multiple comparison post-test vs. control group). 1. Untreated Control, 2. AuNP-C225-gem-mPEG (ACGP), 3. RF alone, 4. AuNP-IgG-gem-mPEG, 5. AuNP-C225-gem-mPEG + RF. N=Necrosis*